Supplementary Information

Systematic change in global patterns of streamflow following volcanic eruptions

Carley E. Iles and Gabriele C. Hegerl

Introduction

In Section 1, Table S1 details the eruptions used in the analysis and the year taken as "year 1" for each. Figure S1 shows volcanic forcing time series since 1850. In Section 2, Table S2 details the CMIP5 runs used to examine the model simulated precipitation response to eruptions. In Section 3 the effect of dams on streamflow is discussed, with Figure S2 illustrating the most extreme case- the effect of the Aswan dam on Nile flow. Section 4 provides further information about the observational river records used: Figure S3 shows the drainage basins used in the study and their regional groupings. Figure S4 shows the rivers used to represent the wet regions. Figure S5 shows the time series for all rivers with the timing of eruptions indicated. Table S3 provides further information for each river, including location of gauging station, annual mean discharge, basin size, record lengths, flow regulation indices and notes on any inhomogeneities. Section 5, shows results for individual years following eruptions: Figure S6 for the CMIP5 simulated precipitation response to eruptions and Figure S7 for observed streamflow. In Section 6, Figure S8 demonstrates that over most regions, precipitation minus evaporation (P-E) is very similar to the precipitation response, using the example of the climate model HadCM3 (pattern correlation of 0.88). This justifies the use of P when determining regions of positive or negative expected streamflow response to volcanism before averaging streamflow across those regions.

Sensitivity of results to differences in analysis method are examined in Section 7. Firstly the influence of ENSO on results is examined: the effect of ENSO on streamflow is shown in Figure S9, and the sensitivity of results in the body of the paper to not removing ENSO is shown in Figures S10 and S11 and Table S4. Figure S12 shows the remaining two regional responses to volcanism for North America and Southern Europe. Figure S13 demonstrates the robustness of regional results to aggregating streamflow across large regions by adding absolute streamflow across rivers, rather than averaging standardized values as in the body of the paper.

Finally, in Section 8 sensitivity to differences in the latitudinal distribution of aerosols between eruptions is discussed. Figure S14 shows the CMIP5 simulated precipitation response to individual eruptions. Table S5 shows the pattern correlations between these precipitation response patterns both between eruptions, and between each eruption and the mean across the remaining eruptions. Finally Figure S15 shows the sensitivity of results for the wet regions to removing the 1912 high latitude eruption.

1. Eruptions used in the analysis

Table S1: Eruption dates and year 1 definitions. Eruption dates and locations are taken from the Global Volcanism Project http://www.volcano.si.edu/world/largeeruptions.cfm. All eruptions are low-latitude except the 1912 Novarupta eruption.

Eruption date	Volcano and location	Start month of year 1	Number of rivers with data
Mid August 1883	Krakatau, Indonesia 6.10°S, 105.42°E	Dec 1883	4
24 Oct 1902	Santa Maria, Guatemala 14.76°N, 91.56°W	Feb 1903	9
6 June 1912	Novarupta, Alaska 58.27°N, 155.16°W	Oct 1912	12
Mid-March 1963	Agung, Indonesia 8.34°S, 115.51°E	July 1963	47
28 March 1982	El Chichon, Mexico 17.36°N, 93.23°W	July 1982	49
15 June 1991	Pinatubo, Philippines 15.13°N, 120.35°E	Oct 1991	46
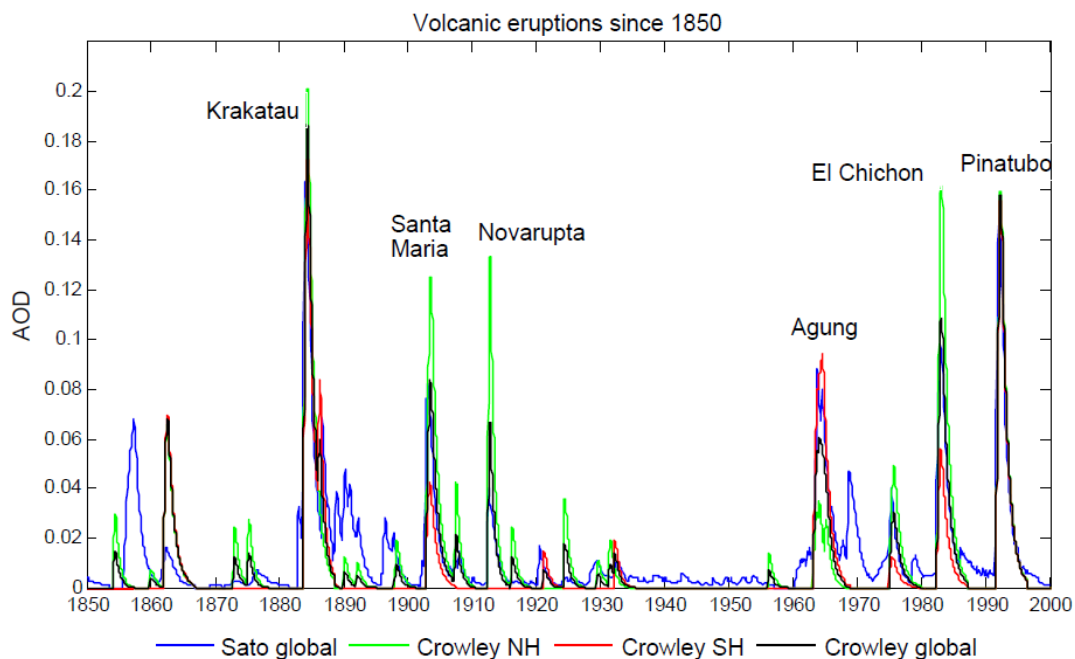
Figure S1: **Aerosol Optical Depth (AOD) since 1850.** *Sato et al.* [1993][8] global mean AOD (blue) and *Crowley et al.*, [2008][43] global mean (black), northern hemisphere mean (green), and southern hemisphere (red).

2. CMIP5 Data

Table S2: CMIP5 runs used.

| Model Name	No. runs	Volcanic forcing dataset	Reference
ACCESS1.0	1	*Sato et al.* [1993][8]	*Bi et al.* [2013][9] *Dix et al.* [2013][10]
ACCESS1.3	1	*Sato et al.* [1993][8]	*Bi et al.* [2013][9] *Dix et al.* [2013][10]
BCC-CSM1.1	3	*Ammann et al.* [2003][11]	*Wu et al.* [2008] [12] *Wu et al.* [2010][13] *Xin et al.* [2013][14]
BNU-ESM	1	*Ammann et al.* [2003][11]	*Feng et al.* [2013][15]
CCSM4	6	*Ammann et al.* [2003][11]	*Gent et.al.* [2011][16] *Meehl et al.* [2012][17]
CNRM-CM5	10	*Ammann et al.* [2007][18]	*Voldoire et al.* [2012][19]
CSIRO-Mk3.6.0	10	*Sato et al.* [1993][8]	*Jeffrey et al.* [2013][20] *Gordon et al.* [2002, 2010][21,22]
CanESM2	5	*Sato et al.* [1993][8]	*Chylek et al.* [2011][23] *Scinocca et al.* [2008][24]
EC-EARTH	5	*Sato et al.* [1993][8]	*Koenigk et al.* [2012][25] *Hazeleger et al.* [2012][26]
GFDL-CM2.1	10	*Sato et al.* [1993][8], *Stenchikov et al.* [1998][27]	*Delworth et al.* [2006][28]
GFDL-CM3	5	*Sato et al.* [1993][8], *Stenchikov et al.* [1998][27]	*Donner et al.* [2011][29]
GISS-E2-H	5	*Sato et al.* [1993][8]	*Schmidt et al.* [2006][30] *Shindell et al.* [2013][31]
GISS-E2-R	6	*Sato et al.* [1993][8]	*Schmidt et al.* [2006][30] *Shindell et al.* [2013][31]
HadCM3	10	*Sato et al.* [1993][8]	*Collins et al.* [2001][32]
HadGEM2-ES	4	*Sato et al.* [1993][8]	*Jones et al.* [2011][33] *Collins et al.* [2011][34]
MIROC5	5	*Sato et al.* [1993][8]	*Watanabe et al.* [2010][35]
MPI-ESM-MR	3	*Stenchikov et al.* [1998][27]	*Schmidt et al.* [2013][36] *Giorgetta et al.* [2013][37]
MRI-CGCM3	5	GEIA[a] [*Andres and Kasgnoc,* 1998][38]	*Yukimoto et al.* [2012][39]
NorESM1-M	3	*Ammann et al.* [2003][11]	*Bentsen et al.* [2013][40] *Iversen et al.* [2012][41]

[a]Global Emissions Inventory Activity database

3. The influence of dams on streamflow

Dams have been found to affect seasonality of streamflow, for instance by increasing winter low flow and reducing spring or summer peak flow in high latitude basins that are influenced by storage of water in snow and ice[1]. Nevertheless, for most rivers dams seem to have little influence on annual flow compared to climate variations[1-3]. However, there are river basins, particularly in dry regions, where flow has decreased due to high levels of regulation by dams and irrigation, which increase water loss by evaporation. Interbasin transfers of water have also contributed to decreased flow for some rivers[3]. Flow regulation indices (live capacity of all the dams on a river, excluding bottom water that cannot be released, as a percentage of annual discharge) for each river are shown in Table S3. Since annual flow is used here, rather than seasonal, the influence of dams should not be problematic for most rivers. Nevertheless, the monthly and annual time series of flow for each river have been examined for possible dam related inhomogeneities, and notes added to Supplementary Table S3. Where monthly flow regimes undergo a discontinuity over time but annual variability and mean discharge do not, this was not considered problematic. However, where annual variability changes drastically post-dam construction such that streamflow variations no longer reflect climate variability, some of the data were disregarded. The most extreme case of this for the rivers used here is the Nile post-Aswan Dam construction (Supplementary Fig. S2). In this case post-Aswan dam data were not used (i.e. 1960 onwards). Other rivers did not show such an extreme change, although some data were also excluded from the Sao Francisco. An inhomogeneity that occurs during a period in which there are no eruptions will not affect the average volcanic response, but will affect confidence intervals obtained through Monte Carlo analysis. Finally, the construction of a large reservoir at the time of an eruption could also be problematic if it causes a temporary reduction in flow whilst the reservoir fills. Here regional results in which several rivers are combined were repeated excluding highly regulated rivers. It was assumed that irrigation has less of a confounding influence on results since it should affect long term trends and intra-annual variability more than interannual variability.
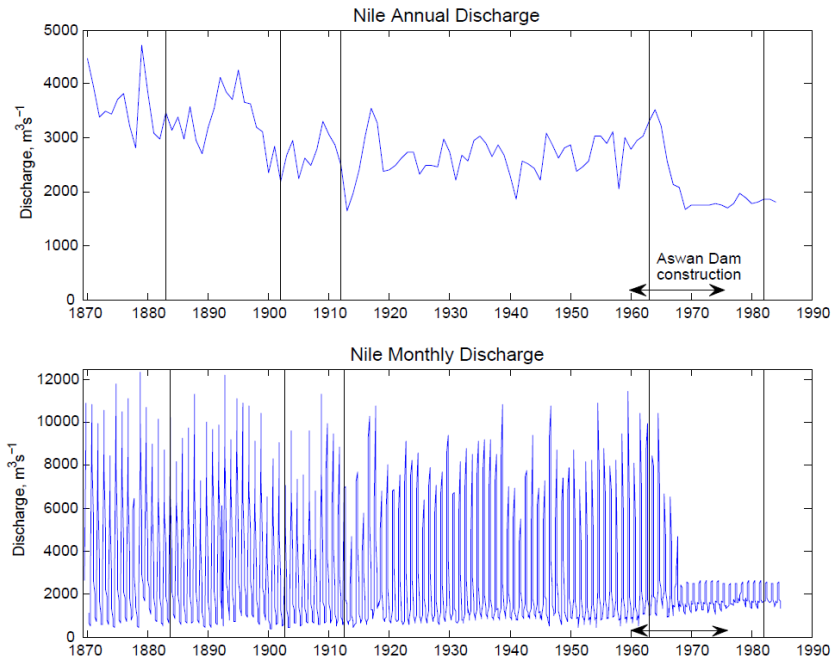
Figure S2: Effects of Aswan Dam on Nile flow. Annual (top) and monthly (bottom) discharge for the Nile River for a station near the Aswan Dam. Vertical lines denote timing of eruptions. Horizontal arrow indicates the time period over which the dam was built: construction commenced in January 1960, the first dam construction phase was finished in 1964 and the reservoir started filling, the High Dam was completed in July 1970 and the reservoir finished filling in 1976. There is a clear change in flow regime before and after dam construction in both monthly and annual data.

4. Rivers used in this study
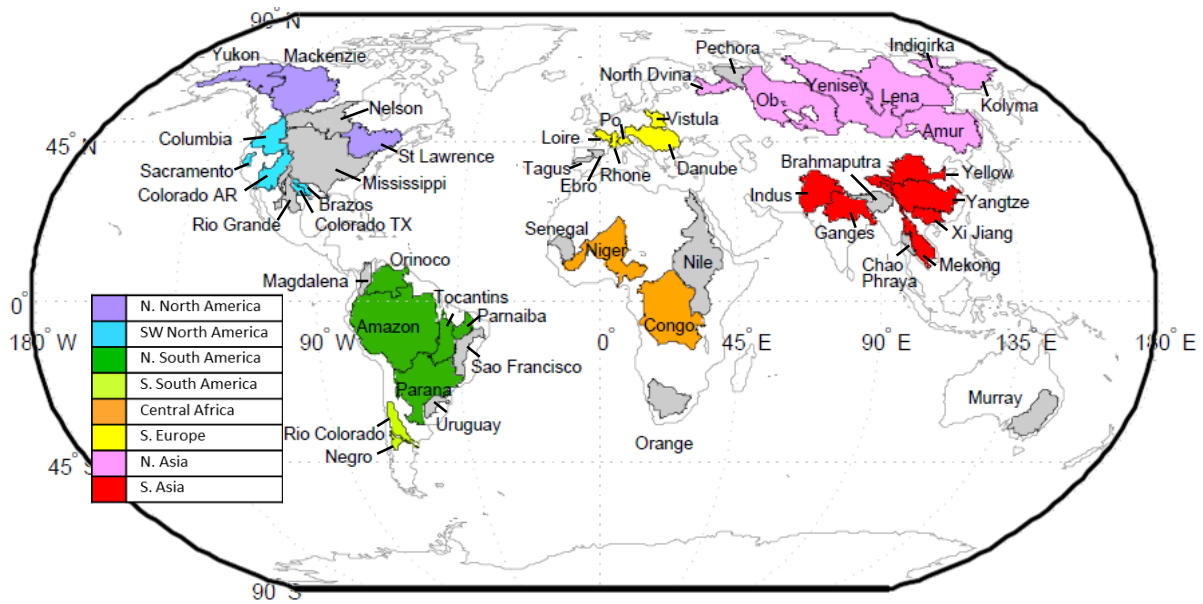
Figure S3: Drainage basins used in this study. Colours indicate the region to which basins are allocated for the regional analysis.
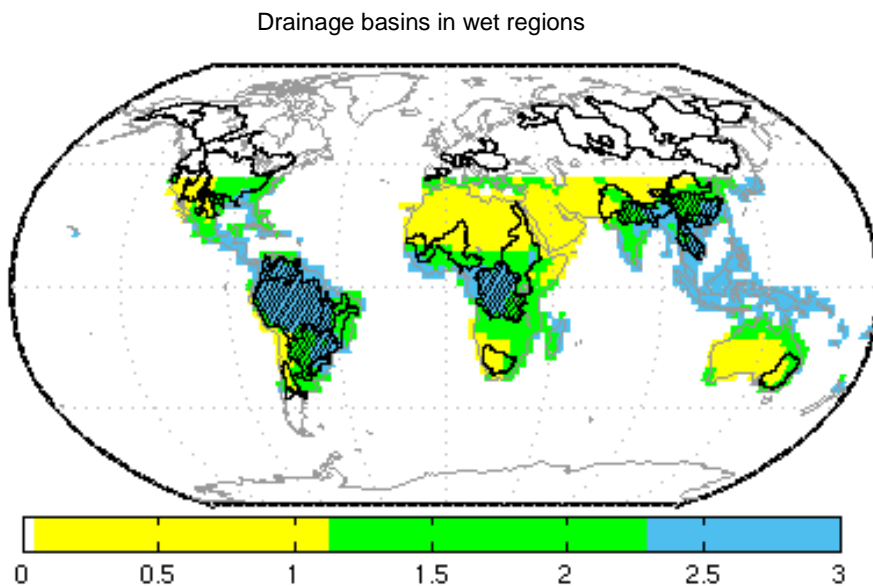
Figure S4: Rivers representing the wet tropical and subtropical regions. Wet (blue), intermediate (green) and dry (yellow) tropical-subtropical regions based on GPCC precipitation climatology with drainage basins overlaid (Wet regions are defined as the wettest third of grid cells between 40°N-40°S, dry regions are the driest third, and intermediate regions, the remaining third). Hatching indicates the basins used to calculate results for the wet regions.
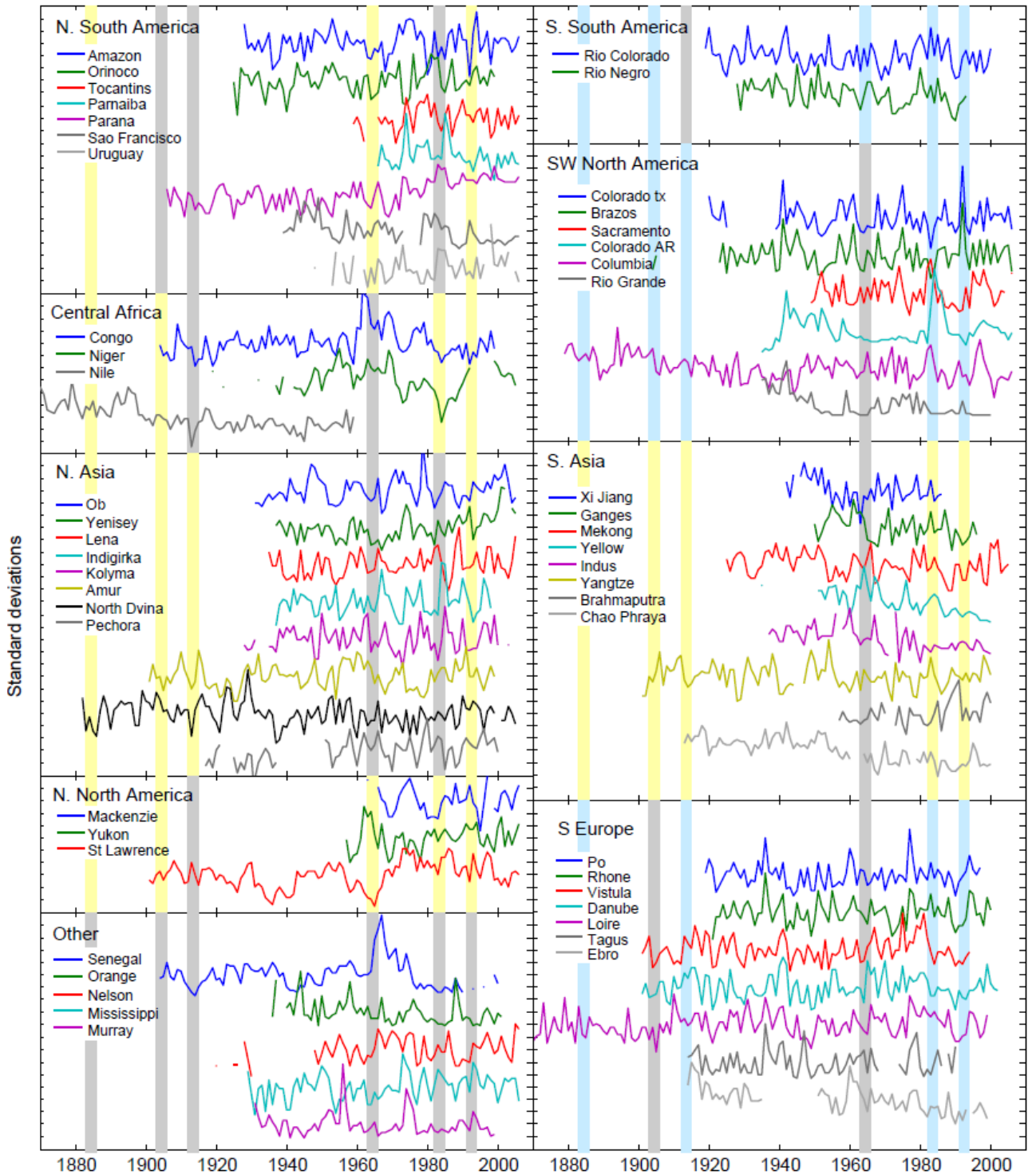
Figure S5: Observed time series of rivers used. Observed annual time series of discharge for all rivers considered in the analysis grouped by regions and expressed in standard deviations. Rivers shown in grey could not be incorporated into the regional analysis because of data coverage limitations (see Methods). Vertical bars denote timing of eruptions, yellow for when CMIP5 simulated precipitation over a given region for a given eruption generally decreases, grey for a mixed signal and blue for a general increase. Rivers under the heading "other" did not fit into a region. Tick mark spacing is 1 standard deviation.

Table S3: Details of the rivers used in the analysis. Rivers with regulation indexes higher than 20% or with inhomogeneities noted are highlighted pink. Flow regulation index data are taken from *Nilsson et al.* [2005][42] and represent the amount of water that can be held in all the dams in a river, expressed as a percentage of annual mean discharge. It uses the dams' 'live capacity', i.e. excluding bottom water that cannot be released, rather than gross capacity.

River name	Region assigned to (see Fig S3)	Station location (lat°N lon°E)	Annual mean discharge at station (km³yr⁻¹) (*and as % of flow at mouth*)[a]	Drainage area at station (10³km²) (*and as % of area at mouth*)[a]	Start Year of record	End Year	No. years data	Eruptions covered	Regulation Index (live dam capacity as % of annual discharge)	Notes (actual data range used and any inhomogeneities)
North America										
Mackenzie	N. North America	67.46 °N, -133.74 °E	283.4 (99.3%)	1660 (96.9%)	1943	2006	46.58	1982, 1991	12	Used from 1964, little data beforehand
Saint Lawrence	N. North America	45 °N, -74.74 °E	224.7 (62.3%)	773.9 (61.1%)	1900	2006	106.75	1902, 1912, 1963, 1982, 1991	11	
Yukon	N. North America	61.93 °N, -162.88 °E	227.5 (95.8%)	831.4 (97.6%)	1956	2006	50	1963, 1982, 1991	0.05	
Columbia	SW North America[b]	45.61 °N, -121.17 °E	164.9 (68.3%)	613.8 (84.8%)	1878	2006	128.25	1883, 1902, 1912, 1963, 1982, 1991	24	
Colorado AR	SW North America	36.02 °N, -114.74 °E	12.4 (108.6%)	444.7 (55%)	1934	2006	72.5	1963, 1982, 1991	280	Unusually high flow around early 1980 to mid-1980s.
Brazos	SW North America	29.58 °N, -95.76 °E	6.7 (94.4%)	116.6 (93.3%)	1903	2006	87.5	1963, 1982, 1991		Used from 1922, large gap before
Colorado TX	SW North America	29.31 °N, -96.1 °E	2.6 (100%)	108.8 (89.9%)	1919	2006	74.67	1963, 1982, 1991		Used from 1938, large gap before
Sacramento	SW North America	38.46 °N, -121.5 °E	21.5 (30.3%)	60.9 (31.5%)	1948	2006	57	1963, 1982, 1991	49	Used up until 2004- missing data afterwards
Nelson	-	54.77 °N, -97.92 °E	69.6 (55.6%)	997 (95.2%)	1915	2006	71.25	1963, 1982, 1991	90	Used from 1947, very incomplete beforehand
Mississippi	-	32.31 °N, -90.91 °E	537.3 (87.9%)	2896 (90.4%)	1928	2006	79	1963, 1982, 1991	15.5	
Rio Grande	-	25.88 °N, -97.45 °E	1.5 (100%)	456.7 (56.7%)	1934	2000	67	1963, 1982, 1991	49	Steep downward trend of discharge until mid-1950s and low flow thereafter

[a] Note that a gauging station only captures streamflow originating from precipitation falling upstream of the station. Therefore it represents an area smaller than the whole drainage basin unless it is located at the river mouth. [b] Although the Columbia is too far North to really be considered as SW North America, and the Brazos and Colorado TX drain into the East Coast, they are all part of a general area experiencing increased precipitation post-eruption that can be best described as SW North America.

River	Region	Location	Annual discharge	Drainage basin area	Start year	End year	No. yrs data	Eruptions	Regulation index	Notes
South America										
Amazon	N. South America	-1.95 °N, -55.51 °E	5389.5 (80.2%)	4618.8 (78.9%)	1928	2006	79	1963, 1982, 1991	3	
Orinoco	N. South America	8.15 °N, -63.6 °E	980.1 (87.2%)	836 (80.5%)	1923	1999	75.75	1963, 1982, 1991	3	Limited data for first 2 years, used from 1925 onwards
Tocantins	N. South America	-3.76 °N, -49.67 °E	357.7 (69.7%)	742.3 (96.5%)	1956	2006	49.42	1982, 1991		Used from 1965 onwards, incomplete record beforehand
Parnaiba	N. South America	-3.46 °N, -42.37 °E	24.0 (92.3%)	282 (85.2%)	1963	2006	43.25	1982, 1991	10	Used from1965, incomplete beforehand
Parana	N. South America	-32.67 °N, -60.71 °E	476.6 (83.8%)	2346 (88.2%)	1905	2006	101.25	1912, 1963, 1982, 1991	28	
Rio Colorado	S. South America	-38.82 °N, -64.95 °E	4.2 (100%)	22.3 (100%)	1918	2000	82.5	1963, 1982, 1991		
Negro	S. South America	-40.45 °N, -63.72 °E	26.9 (93.1%)	95 (48%)	1927	1994	66.83	1963, 1982, 1991	140	Temporarily reduced variability particularly of seasonal flow in early 70s, coinciding with the building of the Palmar dam.
Sao Francisco	-	-9.98 °N, -36.99 °E	89.4 (98.9%)	622.6 (101.2%)	1926	2006	76.42	1963, 1982, 1991	37	Noticeably lower mean annual flow before 1938, data before 1938 not used. Monthly discharge also changes noticeably in its variability after late 1990s.
Uruguay	-	-31.4 °N, -58.03 °E	166.9 72.4(%)	249.3 (70%)	1942	2006	57.25	1963, 1982, 1991	28	Used from 1961, incomplete data before
Magdalena	-	10.25 °N, -74.92 °E	230.9 (100%)	257.4 (102.2%)	1950	2000	51	1963, 1982, 1991	1	
Africa										
Congo	Central Africa	-4.3 °N, 15.3 °E	1270.2 (97.2%)	3475 (93.9%)	1903	2000	97.08	1912, 1963, 1982, 1991	0	
Niger	Central Africa	7.8 °N, 6.77 °E	180.5 (98.6%)	2209.3 (98.6%)	1915	2006	73	1963, 1982, (1991)	15	1991 eruption is used for analysis on the Niger on its own, but not for the regional analysis. Data between 1941-1993 are used, incomplete before and after.
Senegal	-	16.52 °N, -15.5 °E	21.7 (100%)	268 (31.6%)	1903	2000	94.67	1912, 1963, 1982	24	Unusually high flow in late 1960s and early 1970s, returning to normal afterwards.
Orange	-	-28.78 °N, 17.63 °E	6.9 (100%)	850.5 (90.1%)	1935	2001	65.17	1963, 1982, 1991	14	Change in monthly variability in last half of record, not noticeable in annual data.

River	Region	Location	Annual discharge	Drainage basin area	Start year	End year	No. yrs data	Eruptions	Regulation index	Notes
Nile	-	23.96 °N, 32.9 °E			1869	1984	115.17	1883, 1902, 1912	95	Substantial decrease in variability for both annual, but especially monthly flow, along with lower mean flow after construction of the Aswan dam commenced in the 1960s. Post-Aswan dam data are therefore excluded from the analysis.
Europe										
Danube	S. Europe	45.22 °N, 28.73 °E	203.7 (100%)	807 (102.4%)	1900	2002	103	1902, 1912, 1963, 1982, 1991	4.6	
Rhone	S. Europe	43.81 °N, 4.64 °E	53.9 (100%)	95.6 (96.6%)	1920	2000	81	1963, 1982, 1991	5.5	
Loire	S. Europe	47.38 °N, -0.83 °E	27.6 (92.9%)	110 (93.2%)	1863	1999	137	1883, 1902, 1912, 1963, 1982, 1991	1.5	
Po	S. Europe	44.88 °N, 11.65 °E	47.7 (87.3%)	70.1 (68.7%)	1918	1998	80.25	1963, 1982, 1991	4	
Vistula	S. Europe	54.09 °N, 18.8 °E	32.9 (97.1%)	194 (107.2%)	1900	1994	94	1902, 1912, 1963, 1982, 1991	4	
Ebro	-	40.82 °N, 0.5 °E	14.8 (100%)	84.2 (101.5%)	1913	1999	72	1963, 1982, 1991	23	No data between 1936 and 1950
Tagus	-	39.47 °N, -8.37 °E	10.0 (100%)	67.5 (92.5%)	1913	1990	72	1963, 1982	25	
N. Eurasia										
Ob	N. Asia	66.63 °N, 66.6 °E	396.1 (96.4%)	2430 (94.6%)	1930	2006	76	1963, 1982, 1991	9	
Yenisey	N. Asia	67.43 °N, 86.48 °E	583.8 (96.3%)	2440 (94.5%)	1936	2006	69.33	1963, 1982, 1991	18	Used up until 2002, some gaps at end
Lena	N. Asia	70.68 °N, 127.39 °E	529.3 (99.1%)	2430 (100.5%)	1934	2006	71.42	1963, 1982, 1991	3	
Indigirka	N. Asia	69.57 °N, 147.53 °E	50.4 (92.6%)	305 (94.1%)	1936	1998	62.25	1963, 1982, 1991	0	
Kolyma	N. Asia	68.73 °N, 158.72 °E	97.1 (83.9%)	526 (79%)	1927	2004	74.25	1963, 1982, 1991	5	1934-2001 used, incomplete otherwise
Amur	N. Asia	50.53 °N, 137 °E	305.9 (88.1%)	1730 (59.6%)	1900	1999	99.92	1902, 1912, 1963, 1982, 1991	9	
North Dvina	N. Asia	64.13 °N, 41.92 °E	104.4 (94.6%)	348 (94.8%)	1881	2006	124	1883, 1902, 1912, 1963, 1982, 1991	1	

River	Region	Location	Annual discharge	Drainage basin area	Start year	End year	No. yrs data	Eruptions	Regulation index	Notes
Pechora	-	67.63 °N, 52.18 °E	137.8 (96.4%)	312 (103.3%)	1916	2000	73.75	1963, 1982, 1991	0	First half of record incomplete, so data used from 1950 onwards
S. Asia										
Ganges	S. Asia	24.55 °N, 88.13 °E	379.7 (94.6%)	951 (99.5%)	1949	1996	48	1963, 1982, 1991	8	
Mekong	S. Asia	15.11 °N, 105.8 °E	300.4 (55.6%)	545 (70.4%)	1923	2005	82.58	1963, 1982, 1991	3	Used from 1924
Yellow (Huang He)	S. Asia	35.23 °N, 114.92 °E	44.9 (95.7%)	734.1 (82.1%)	1934	2000	52.33	1963, 1982, 1991	51	Used from 1950, large gap in data beforehand
Xi Jiang (Pearl)	S. Asia	23.48 °N, 111.32 °E	219.7 (81.9%)	329.7 (80.6%)	1915	1986	45.67	1963, 1982	31	Used from 1941 large gap in data beforehand
Yangtze (Chang Jiang)	S. Asia	30.77 °N, 117.62 °E	905.1 (96.4%)	1705.4 (95.1%)	1900	2000	99.58	1902, 1912, 1963, 1982, 1991	12	
Indus	S. Asia	25.36 °N, 68.3 °E	88.5 (85.6%)	975 (85.3%)	1936	2000	63.75	1963, 1982, 1991	13	
Brahmaputra	-	25.18 °N, 89.67 °E	670.9 (97.6%)	554.5 (95.1%)	1956	2000	44.25	1963, 1982, 1991	8	
Chao Phraya	-	15.27 °N, 100.06 °E	23.3 (85.3%)	118.8 (83.7%)	1912	2000	86.5	1963, 1982, 1991	76	Discontinuity in annual mean flow and monthly variability from 1952 after construction of Chao Phraya dam. However, annual variability appears unchanged.
Australia										
Murray Darling	-	-34.6 °N, 142.76 °E	8.5 (90.4%)	991 (96%)	1930	2000	69.92	1963, 1982, 1991	67	

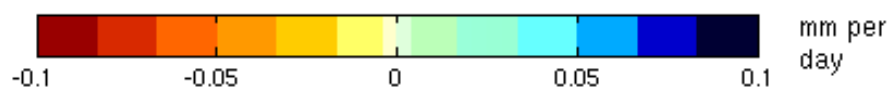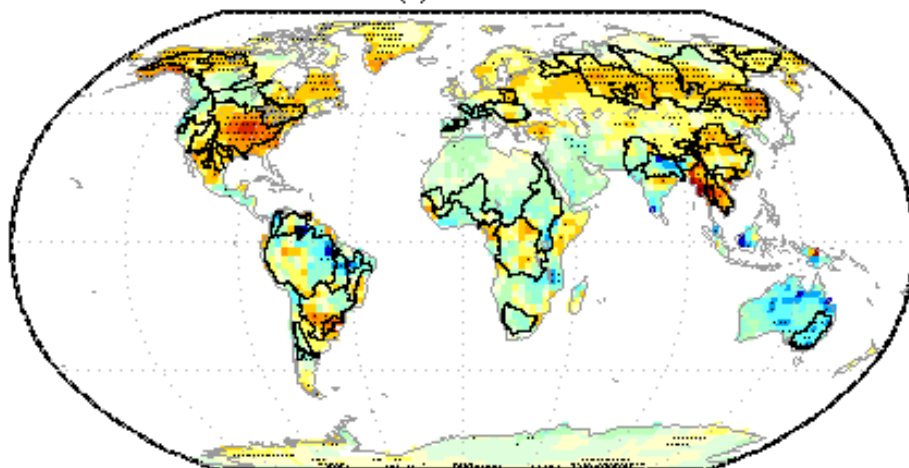**5. Multi-eruption response for individual years following eruptions**
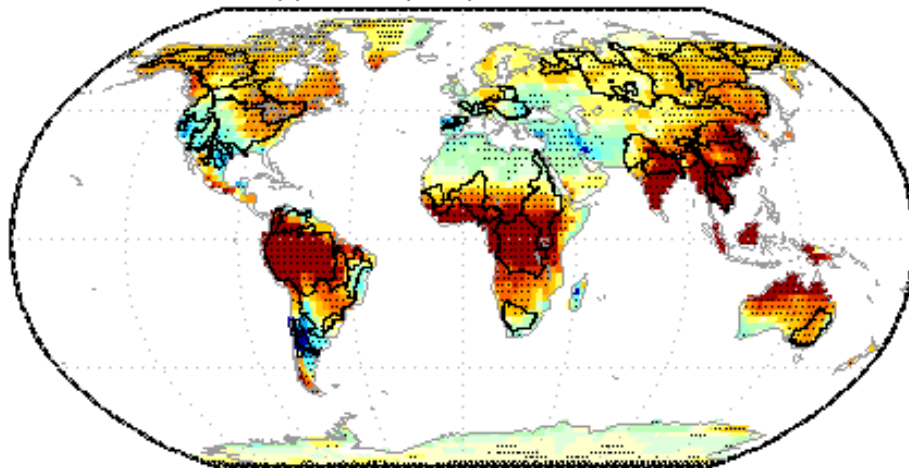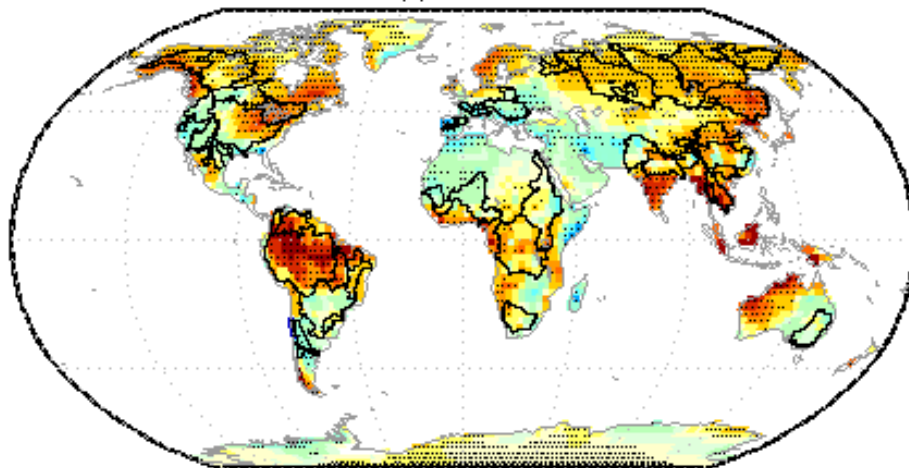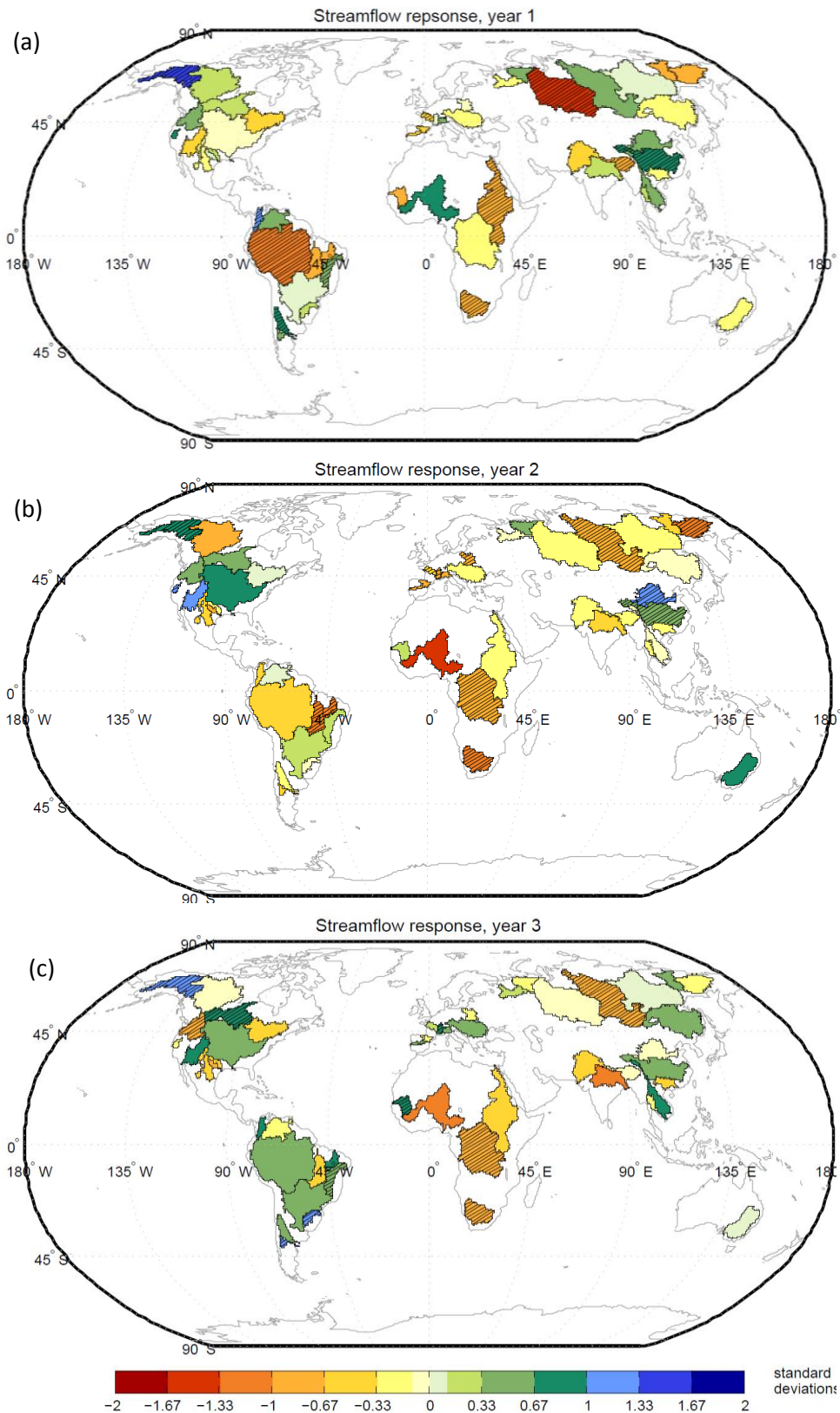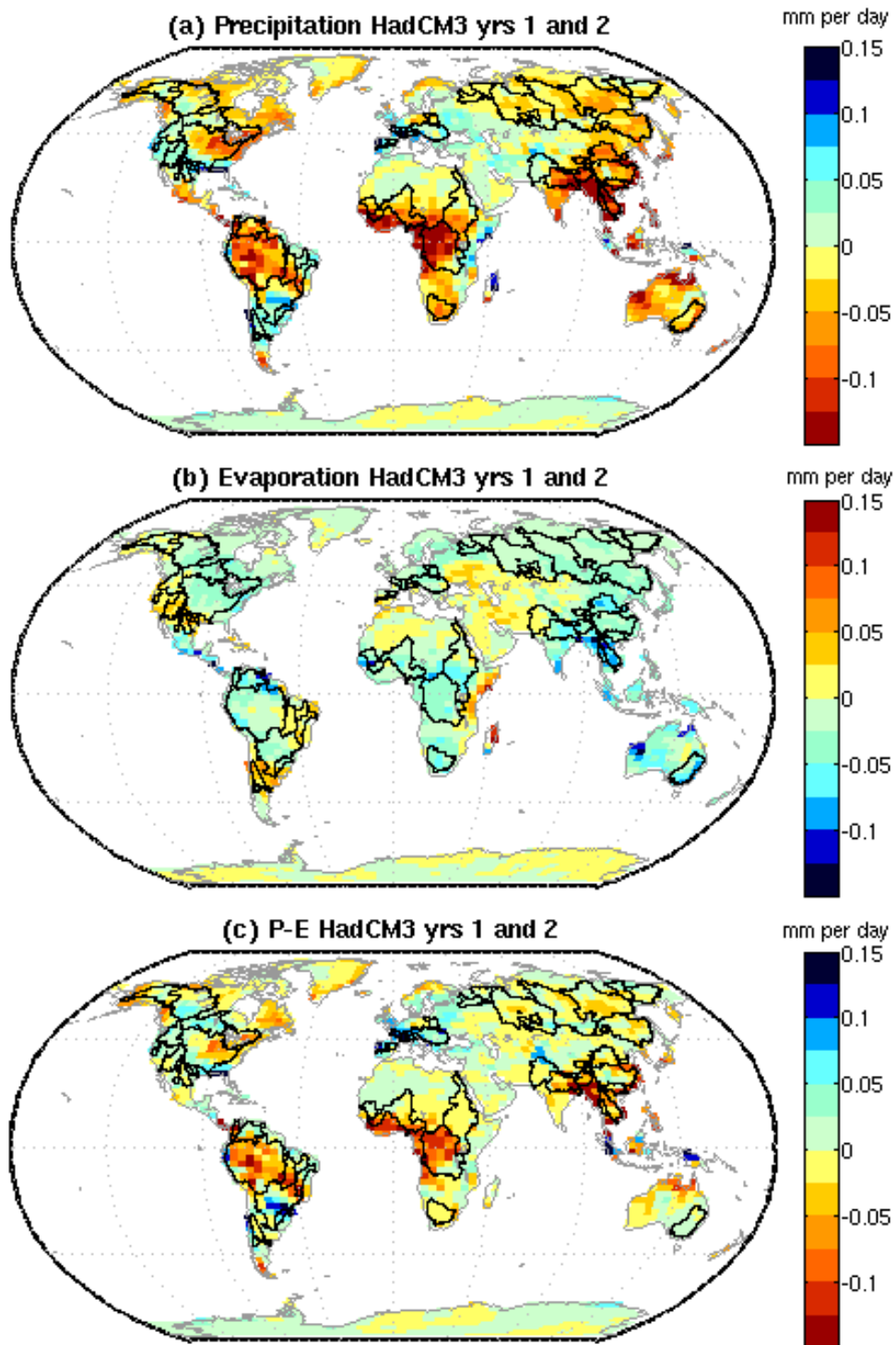

Figure S6: CMIP5 simulated precipitation response to eruptions. As Figure 1a, but for years 1 to 3 separately.

Figure S7: Observed streamflow response to eruptions. As Figure 1c, but for each of the 3 years following eruptions separately. 10% of rivers show a streamflow response in the direction expected from CMIP5 simulated precipitation in yr1, compared to 12% in yr2 and 8% in yr3 (10% significance level).

6. Precipitation, Evaporation and P-E

Figure S8: Model simulated P, E and P-E response to eruptions. Response of a) precipitation, b) evaporation and c) precipitation minus evaporation for the first year following 6 volcanic eruptions in an ensemble of 10 HadCM3 runs (the runs detailed in Supplementary Table S2). Note that the colour scale for evaporation is inverted. The pattern correlation between P and P-E for HadCM3 is 0.88

7. Sensitivity tests

Sensitivity to ENSO removal
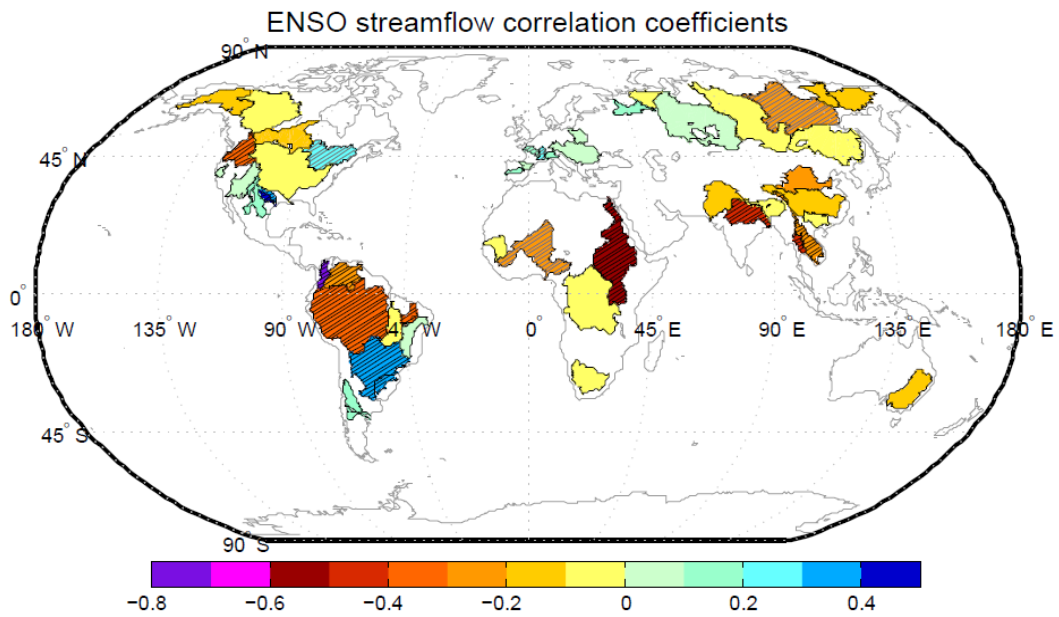
Figure S9: The influence of ENSO on streamflow. Correlation coefficients between ENSO and observed streamflow using water years (Oct-Sept). Hatching indicates a significant relationship (using a white noise assumption), black hatching at the 95% level and grey the 90% level. Note that the length of time series used for the correlation is different for each river depending on its record length (see Table S3).
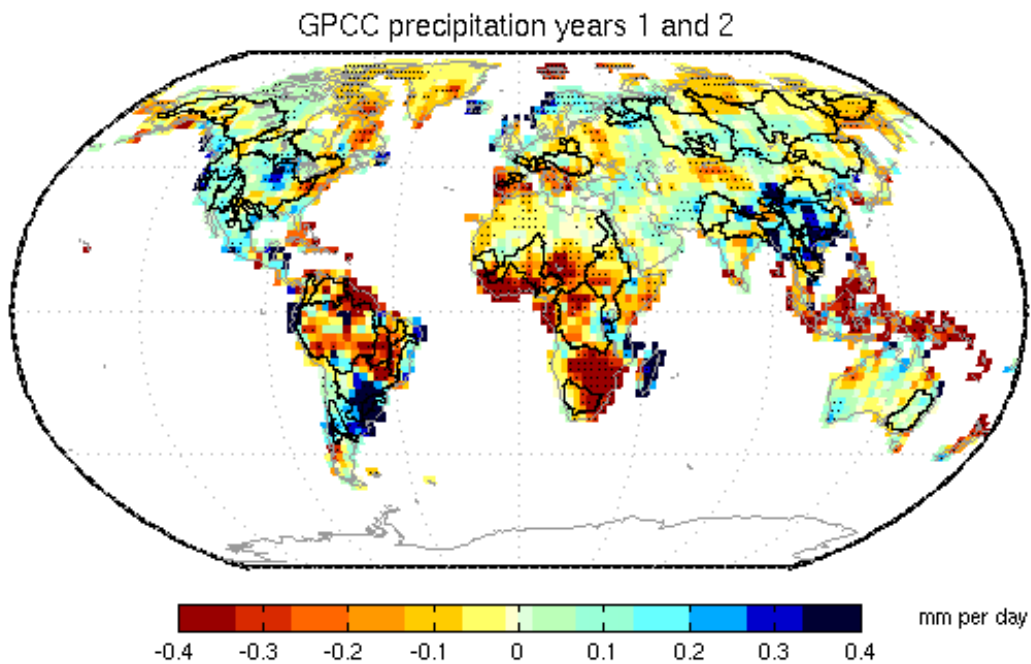
Figure S10: Observed precipitation response to eruptions. As Figure 1c but without ENSO removal.
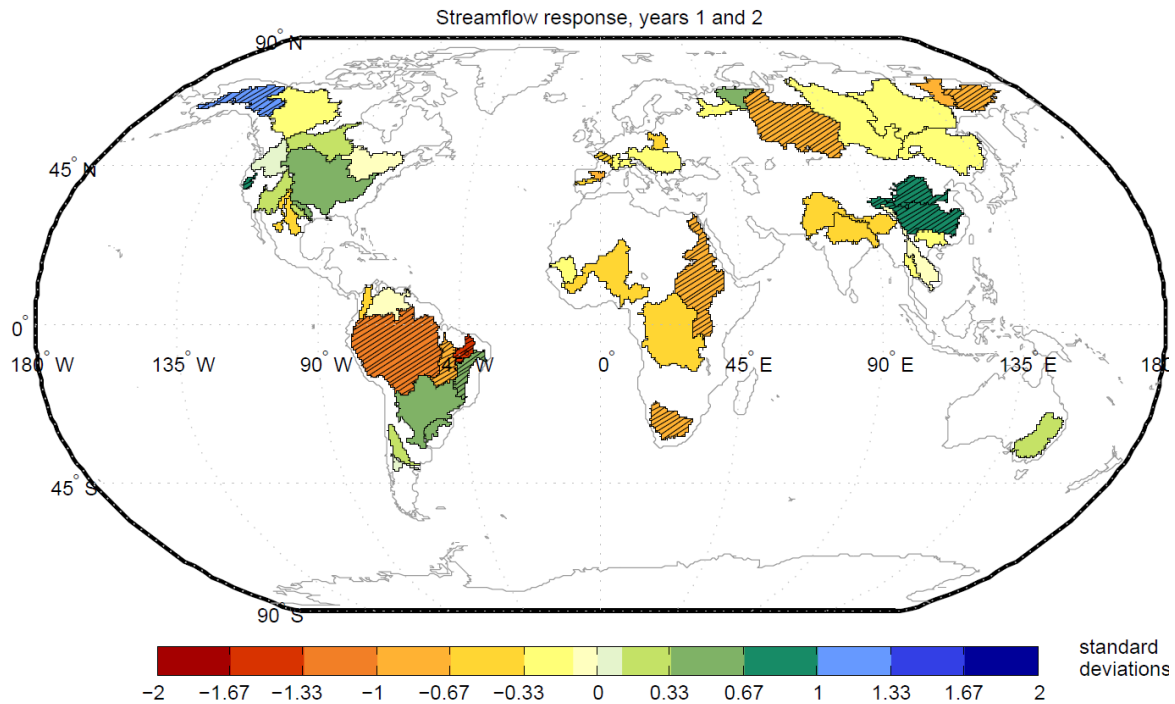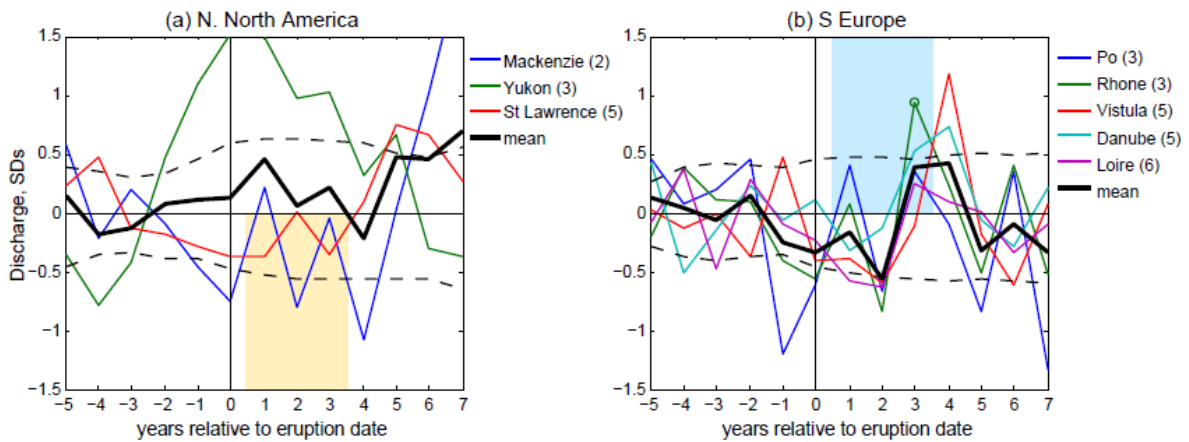
Figure S11: Observed streamflow response to eruptions. As Figure 1b but without ENSO removal. 14% of basins exhibit a significant response in the direction expected from the CMIP5 simulated response of precipitation to eruptions both with and without ENSO removal (10% significance level).

Table S4: Percentage of rivers responding to volcanic eruptions. As Table 1 but without ENSO removal

Basin type (no. rivers)	yr1	yr2	yr3	yrs 1 and 2	Number expected by chance
All (50)	6 (12%)	7 (14%)	5 (10%)	7 (14%)	5 (10%)
All rivers sign. CMIP5 precip (38)	6 (16%)	7 (18%)	4 (11%)	7 (18%)	3.6 (10%)
Natural (22)	4 (18%)	4 (18%)	2 (9%)	4 (18%)	2.1 (10%)
Human (12)	1 (8%)	2 (17%)	2 (17%)	2 (17%)	1.2 (10%)
Big (21)	4 (19%)	5 (24%)	3 (14%)	5 (24%)	2 (10%)
Small (17)	2 (12%)	2 (12%)	1 (6%)	2 (12%)	1.6 (10%)
Regions standardised (8)	3 (37.5%)	3 (37.5%)	1 (12.5%)	2 (25%)	0.8 (10%)
Regions absolute (8)	2 (25%)	1 (12.5%)	2 (25%)	1 (12.5%)	0.8 (10%)

Sensitivity tests for regional results

Figure S12: Observed regional streamflow responses not shown in body of paper. As in Figure 2 but for (a) Northern North America and (b) Southern Europe. Although the CMIP5 simulations suggest that southern Europe should experience increased precipitation after eruptions, the observed decrease in streamflow is consistent with a positive NAO response to eruptions which has been found in observational studies[44,45].
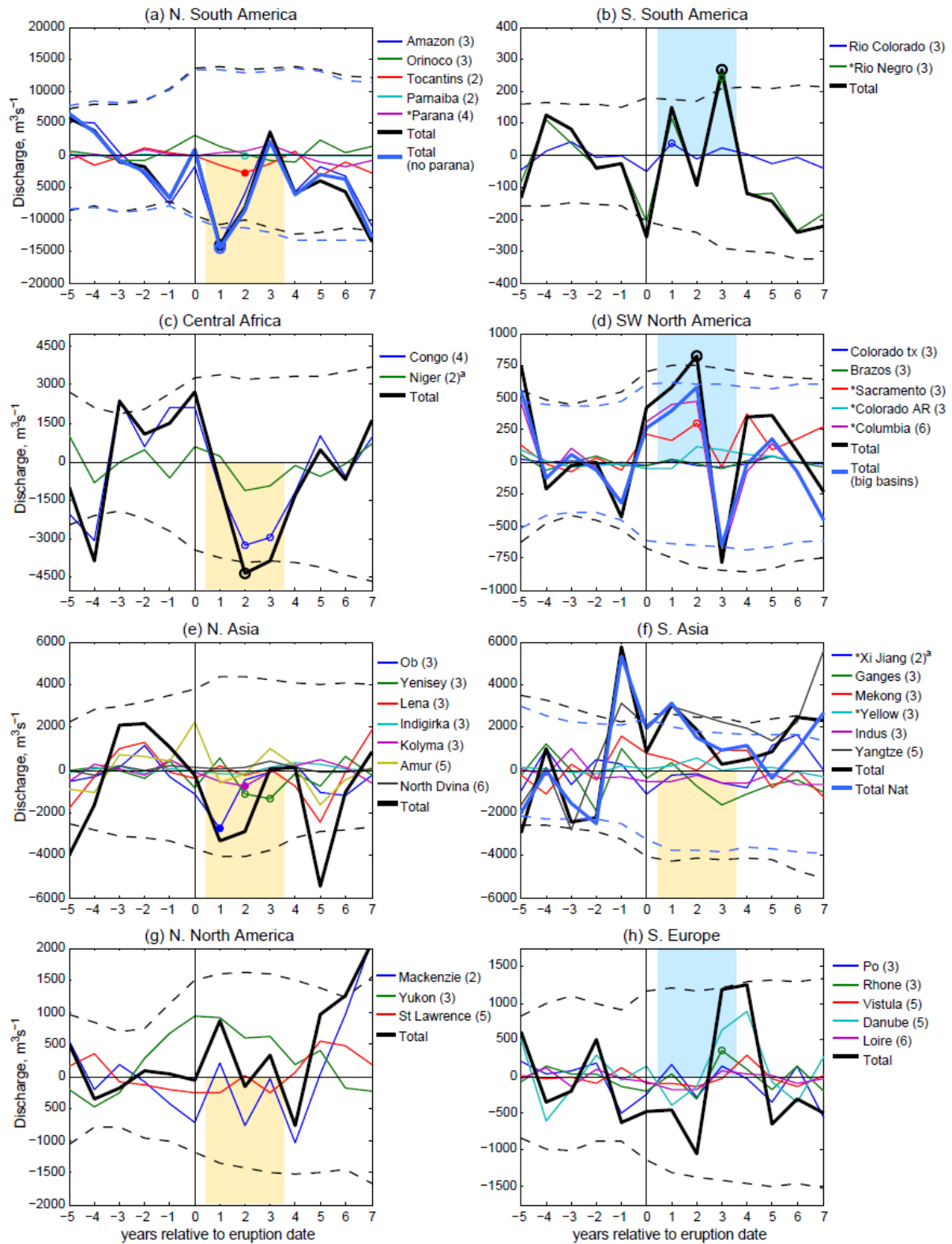
Figure S13: Observed regional streamflow responses. As Figure 2 and S12 but using absolute values (m³/s), aggregating the streamflow response across regions rather than averaging standardized response as in the body of the paper. Thick black and blue lines represent the sum of the epoch results for individual rivers (thin lines).

8. Sensitivity to differences in aerosol cloud latitudinal distribution between individual eruptions

Volcanic aerosols encircle the earth zonally within 2-3 weeks of an eruption. They also spread polewards over the following months, over both hemispheres for tropical eruptions, and over the hemisphere of eruption for high latitude ones[4,5]. However, even for low-latitude eruptions, the aerosol cloud is not always evenly distributed between the hemispheres. Here we investigate the extent to which these differences are likely to affect the level of consistency of the precipitation, and therefore streamflow response between the eruptions used here. This analysis is based on the CMIP5 precipitation response, as the large ensemble allows us to identify differences in response between eruptions which will be at least partially obscured by noise in observations of precipitation and streamflow. Figure S5 also shows expected differences between eruptions for different regions by showing the sign of CMIP5 precipitation response for each eruption and each region.

Figure S1 shows the aerosol distribution between the two hemispheres of the volcanic eruptions used in the analysis. The 1912 Novarupta eruption was a high northern latitude eruption, whilst the rest were tropical. The aerosol clouds following Krakatau (1883) and Pinatubo (1991) were symmetrical between the hemispheres, those of Santa Maria (1902) and El Chichon (1982) were biased towards the northern hemisphere, whilst that of Agung (1963) was southern hemisphere biased.

Figure S14 shows the CMIP5 multi-model mean precipitation response to each eruption separately to give an indication of how much streamflow might be expected to be affected by differences in the latitudinal distribution of aerosols between eruptions. Many features of the precipitation response are similar between eruptions, the main difference being that the ITCZ tends to shift away from the hemisphere that has the largest concentration of aerosols, particularly over ocean[6,7]. The precipitation response over land to the 1883 (symmetrical aerosol cloud), 1902 (NH bias), 1982 (NH bias) and 1991 (symmetrical) eruptions is very similar (see Table S5 for pattern correlations between the precipitation response of individual eruptions and with the mean of the rest of the eruptions).

For the 1912 high latitude eruption (Fig S14c) the main difference from the mean across all eruptions (Fig S14g) is that CMIP5 simulated precipitation over the Amazon and Congo basins increases rather than decreases. The Amazon has no streamflow data for 1912, so this will not affect results. Figure S15 shows the impact of removing the 1912 eruption from the Congo, and from all rivers with data (Congo, Parana, Yangtze) for the wet regions streamflow analysis. Results, particularly using absolute values, are robust to excluding 1912, although become insignificant for the standardised version of the analysis. However, if we only remove the 1912 eruption from the Congo, which is the river within the wet regions that is most likely to be differently affected by 1912 based on Figure S14, results remain almost exactly the same as the original version of the analysis. Globally, 12 rivers used here have data for 1912 compared to 46-49 for the more recent three eruptions, so this eruption will not have a large weight in the results. The CMIP5 simulated precipitation response to Agung (1963) also differs from the

other eruptions (Figure S14), since it is the only eruption whose aerosol cloud is biased towards the southern hemisphere. The main differences is that the ITCZ shifts northwards and the Niger and Nile therefore get wetter instead of drier. The response is also a bit more patchy over SE Asia, SW North America and southern Europe. Elsewhere the precipitation response is consistent with the other eruptions. In the bottom panels of Figure S14 we also show the precipitation response averaged across all 6 eruptions compared to just the most recent three. The patterns are very similar.

In an ideal world with a large sample of eruptions, it would be informative to group eruptions according to their aerosol cloud distribution. However, due to the small number of eruptions covered by most rivers (often 3, one of which is Agung), it was not possible here. Nevertheless, aggregating across slightly different responses should lead to decreased detectability and not spurious detection of responses.
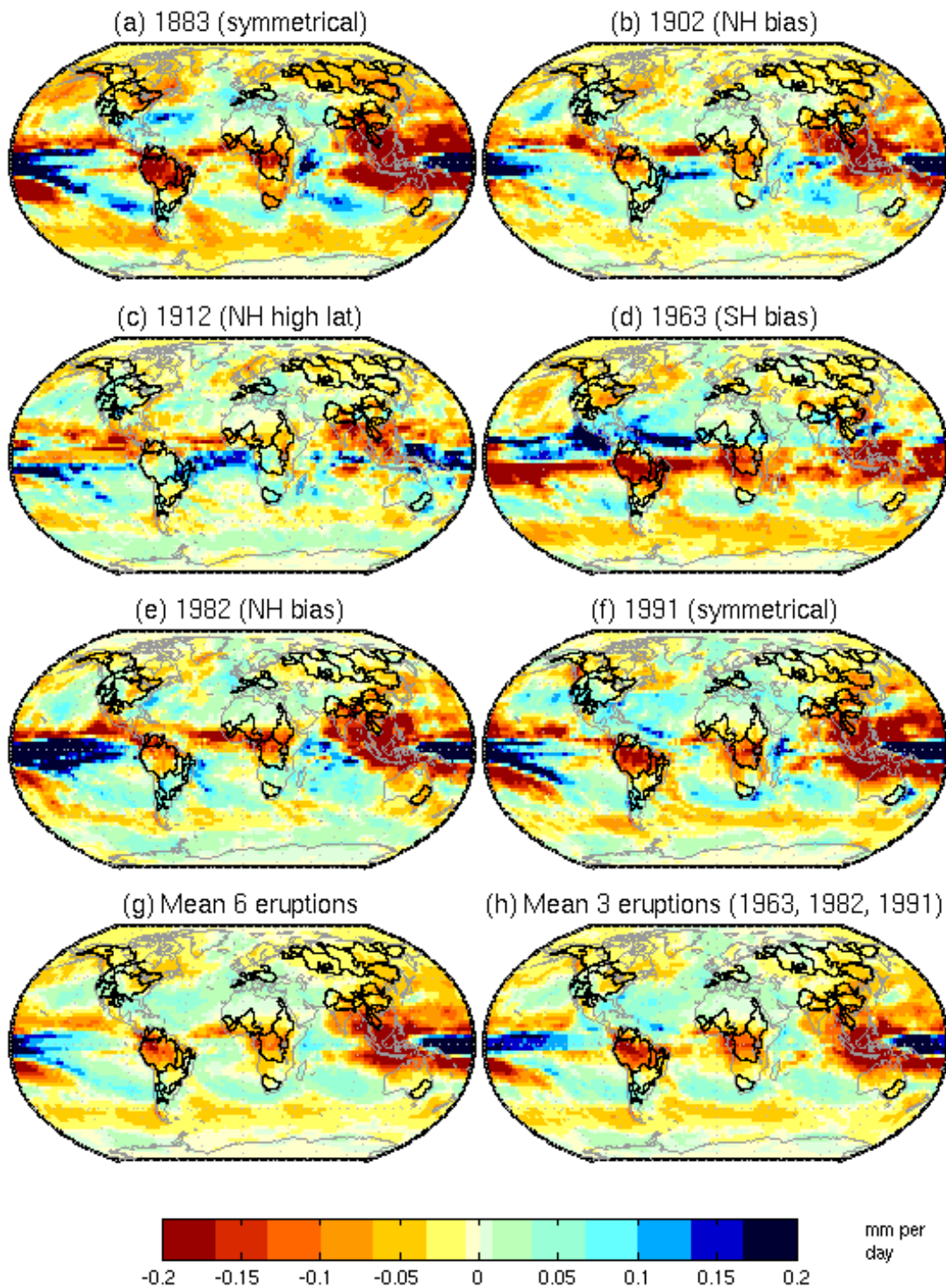
Figure S14: CMIP5 multi model mean precipitation response to individual eruptions. (a) Krakatau, (b) Santa Maria, (c) Novarupta, (d) Agung, (e) El Chichon and (f) Pinatubo. Distribution of the aerosol clouds for each eruption is indicated in brackets (NH is Northern Hemisphere, SH is Southern Hemisphere, "high lat" is high latitude). (g) Mean across all 6 eruptions and (h) across the most recent 3 eruptions [mm per day].

Table S5: Pattern correlations between CMIP5 multi-model mean precipitation response to individual eruptions. Patterns analysed are those in Figure S14. Last column gives the pattern correlation between each eruption and the mean across the remaining eruptions. Values larger than 0.6 are in shaded yellow.

Eruption	1883	1902	1912	1963	1982	1991	Mean of remaining eruptions
1883	1.00	0.71	0.22	0.51	0.72	0.81	**0.85**
1902		1.00	0.41	0.28	0.75	0.65	**0.77**
1912			1.00	-0.23	0.40	0.26	**0.26**
1963				1.00	0.21	0.47	**0.36**
1982					1.00	0.69	**0.76**
1991						1.00	**0.81**
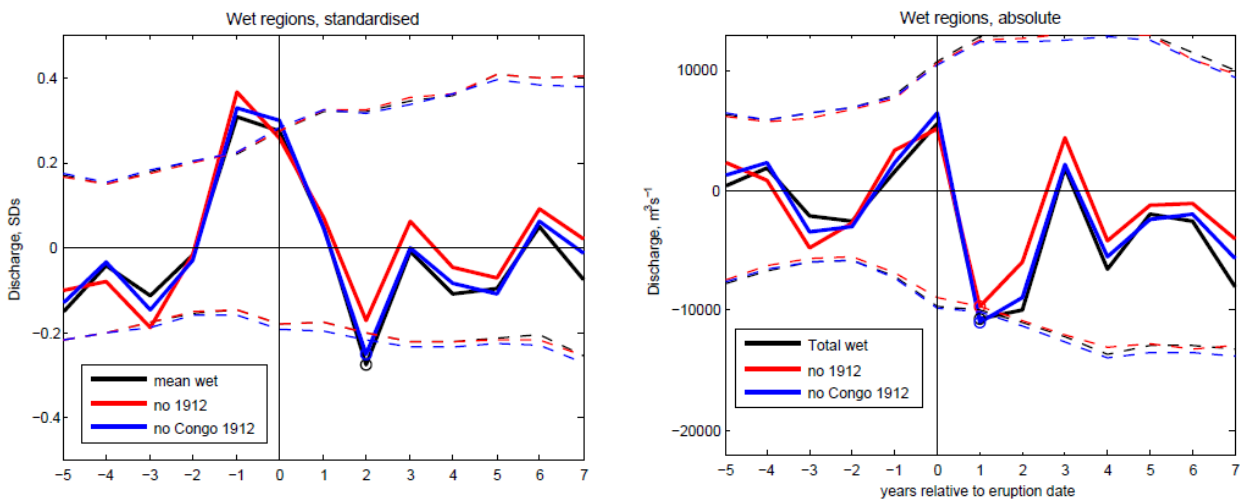
Figure S15: Sensitivity of wet regions response to 1912 eruption. As in Figure 3, but testing sensitivity to removing the 1912 high latitude eruption. Thick black line is the mean (or sum) across all 10 rivers in the wet regions, and is the same as the black lines in Figure 3. Red line is for removing the 1912 eruption from the analysis from all rivers that have data for it (Congo, Parana, and Yangtze). Blue line is for only removing 1912 from the Congo.

References

1. Adam, J. C. & Lettenmaier, D. P. Application of New Precipitation and Reconstructed Streamflow Products to Streamflow Trend Attribution in Northern Eurasia. *Journal of Climate* **21,** 1807–1828 (2008).

2. Dai, A., Qian, T., Trenberth, K. E. & Milliman, J. D. Changes in Continental Freshwater Discharge from 1948 to 2004. *Journal of Climate* **22,** 2773–2792 (2009).

3. Milliman, J. D., Farnsworth, K. L., Jones, P. D., Xu, K. H. & Smith, L. C. Climatic and anthropogenic factors affecting river discharge to the global ocean, 1951–2000. *Global and Planetary Change* **62,** 187–194 (2008).

4. Robock, A. Volcanic eruptions and climate. *Rev. Geophys.* **38,** 191–219 (2000).

5. Timmreck, C. Modeling the climatic effects of large explosive volcanic eruptions. *Wiley Interdiscip. Rev. Clim. Chang.* **3,** 545–564 (2012).

6. Haywood, J. M., Jones, A., Bellouin, N. & Stephenson, D. Asymmetric forcing from stratospheric aerosols impacts Sahelian rainfall. *Nat. Clim. Chang.* **3,** 660–665 (2013).

7. Iles, C. E. & Hegerl, G. C. The global precipitation response to volcanic eruptions in the CMIP5 models. *Environmental Research Letters* **9,** 104012 (2014).

8. Sato, M., Hansen, J. E., McCormick, M. P. & Pollack, J. B. Stratospheric aerosol optical depths, 1850-1990. *J. Geophys. Res.* **98,** 22987–22994 (1993).

9. Bi, D. *et al.* The ACCESS coupled model: Description, control climate and evaluation. *Aust. Meteorol. Ocean* **63,** 41–64 (2013).

10. Dix, M. *et al.* The ACCESS Coupled Model: Documentation of core CMIP5 simulations and initial results. *Aust. Meteorol. Ocean.* **63,** 83–99 (2013).

11. Ammann, C. M., Meehl, G. A., Washington, W. M. and Zender, C.S. A monthly and latitudinally varying volcanic forcing dataset in simulations of 20th century climate. *Geophys.Res. Lett.* **30,** 1657 (2003).

12. Wu, T., Yu, R. & Zhang, F. A Modified Dynamic Framework for the Atmospheric Spectral Model and Its Application. *J. Atmos. Sci.* **65,** 2235–2253 (2008).

13. Wu, T. *et al.* The Beijing Climate Center atmospheric general circulation model: description and its performance for the present-day climate. *Clim. Dyn.* **34,** 123–147 (2010).

14. Xin, X. G. *et al*. How well does BCC_CSM1. 1 reproduce the 20th century climate change over China? *Atmos. Oceanic Sci. Lett* **6,** 21–26 (2013).

15. Feng, J. Introduction of the CMIP5 Experiments Carried out by BNU-ESM. *Advances in Climate Change Research* **9,** 291–294 (2013).

16.   Gent, P. R. *et al.* The Community Climate System Model Version 4. *Journal of Climate* **24,** 4973–4991 (2011).

17.   Meehl, G. A. *et al.* Climate System Response to External Forcings and Climate Change Projections in CCSM4. *Journal of Climate* **25,** 3661–3683 (2012).

18.   Ammann, C. M., Joos, F., Schimel, D. S., Otto-bliesner, B. L. & Tomas, R. A. Solar influence on climate during the past millennium : Results from transient simulations with the NCAR Climate System Model. **104,** 3713–3718 (2007).

19.   Voldoire, A. *et al.* The CNRM-CM5.1 global climate model: description and basic evaluation. *Climate Dynamics* **40,** 2091–2121 (2012).

20.   Jeffrey, S. *et al.* Australia 's CMIP5 submission using the CSIRO-Mk3.6 model. *Aust. Meteorol. Ocean.* **63,** 1–13 (2013).

21.   Gordon, H. B. *et al.* The CSIRO Mk3 climate system model, *Tech. Pap. 60*, Atmos. Res., Commonw. Sci. and Ind. Res. Org.,Aspendale, Victoria, Australia. (2002).

22   Gordon, H. B. *et al.* The CSIRO Mk3.5 Climate Model, technical report no. 21, *Technical Report 021*, CAWCR, Aspendale, Vic., Australia. (2010).

23.   Chylek, P., Li, J., Dubey, M. K., Wang, M. & Lesins, G. Observed and model simulated 20th century Arctic temperature variability: Canadian Earth System Model CanESM2. *Atmospheric Chemistry and Physics Discussions* **11,** 22893–22907 (2011).

24.   Scinocca, J. F., McFarlane, N. A., Lazare, M., Li, J. & Plummer, D. Technical Note: The CCCma third generation AGCM and its extension into the middle atmosphere. *Atmospheric Chemistry and Physics* **8,** 7055–7074 (2008).

25.   Koenigk, T. *et al.* Arctic climate change in 21st century CMIP5 simulations with EC-Earth. *Climate Dynamics* **40,** 2719–2743 (2012).

26.   Hazeleger, W. *et al.* EC-Earth V2.2: description and validation of a new seamless earth system prediction model. *Climate Dynamics* **39,** 2611–2629 (2012).

27.   Stenchikov, L. *et al.* Radiative forcing from the 1991 Mount Pinatubo volcanic eruption. *J. Geophys. Res.* **103,** 13,837–13,857 (1998).

28.   Delworth, T. J. et al. GFDL' s CM2 Global Coupled Climate Models . Part I : Formulation and Simulation Characteristics. *Journal of Climate* **19,** 643–674 (2006).

29.   Donner, L. J. *et al.* The Dynamical Core, Physical Parameterizations, and Basic Simulation Characteristics of the Atmospheric Component AM3 of the GFDL Global Coupled Model CM3. *Journal of Climate* **24,** 3484–3519 (2011).

30.   Schmidt, G. *et al.* Present-day atmospheric simulations using GISS ModelE: Comparison to in situ, satellite, and reanalysis data. *Journal of climate* **19,** 153–192 (2006).

31.   Shindell, D. T. *et al.* Interactive ozone and methane chemistry in GISS-E2 historical and future climate simulations. *Atmospheric Chemistry and Physics* **13,** 2653–2689 (2013).

32.   Collins, M., Tett, S. and Cooper, C. The internal climate variability of HadCM3, a version of the Hadley Centre coupled model without flux adjustments. *Clim. Dyn.,* **17,** 61–68 (2001)

33.   Jones, C. D. *et al.* The HadGEM2-ES implementation of CMIP5 centennial simulations. *Geoscientific Model Development* **4,** 543–570 (2011).

34.   Collins, W. J. *et al.* Development and evaluation of an Earth-System model – HadGEM2. *Geoscientific Model Development* **4,** 1051–1075 (2011).

35.   Watanabe, M. *et al.* Improved Climate Simulation by MIROC5: Mean States, Variability, and Climate Sensitivity. *Journal of Climate* **23,** 6312–6335 (2010).

36.   Schmidt, H. *et al.* Response of the middle atmosphere to anthropogenic and natural forcings in the CMIP5 simulations with the Max Planck Institute Earth system model. *Journal of Advances in Modeling Earth Systems* **5,** 98–116 (2013).

37.   Giorgetta, M. A. *et al.* Climate and carbon cycle changes from 1850 to 2100 in MPI-ESM simulations for the Coupled Model Intercomparison Project phase 5. *Journal of Advances in Modeling Earth Systems* **5,** 572–597 (2013).

38.   Andres, R. J. & Kasgnoc, A. D. A time averaged inventory of subaerial volcanic sulphur emissions. *Journal of Geophysical Research* **103,** 25251–25261 (1998).

39.   Yukimoto, S. *et al.* A New Global Climate Model of the Meteorological Research Institute: MRI-CGCM3-Model Description and Basic Performance. *Journal of the Meteorological Society of Japan* **90A,** 23–64 (2012).

40.   Bentsen, M. *et al.* The Norwegian Earth System Model, NorESM1-M – Part 1: Description and basic evaluation of the physical climate. *Geoscientific Model Development* **6,** 687–720 (2013).

41.   Iversen, T. *et al.* The Norwegian Earth System Model, NorESM1-M – Part 2: Climate response and scenario projections. *Geoscientific Model Development* **6,** 389–415 (2013).

42.   Nilsson, C., Reidy, C. A, Dynesius, M. & Revenga, C. Fragmentation and flow regulation of the world's large river systems. *Science* **308,** 405–8 (2005).

43.   Crowley, T.J. *et al.* Volcanism and the little ice age. *PAGES News* **16,** 22-23 (2008).

44.   Robock, A. & Liu, Y. The volcanic signal in goddard institue for space studies and 3d model simulations. *Journal of Climate* **7,** 44–55 (1994).

45.   Robock, A. & Mao, J. Winter Warming from Large Volcanic Eruptions. *Geophysical Research Letters* **19,** 2405–2408 (1992).